# E-Joint: Fabrication of Large-Scale Interactive Objects Assembled by 3D Printed Conductive Parts with Copper Plated Joints


Xiaolong Li*
Zhejiang University
Hangzhou, Zhejiang, China
lixiaolong@zju.edu.cn

Cheng Yao*
Zhejiang University
Hangzhou, Zhejiang, China
yaoch@zju.edu.cn

Shang Shi
Zhejiang University
Hangzhou, Zhejiang, China
shishang@zju.edu.cn

Shuyue Feng
Zhejiang University
MIT CSAIL
Cambridge, MA, USA
shuyuefeng@zju.edu.cn

Yujie Zhou
Zhejiang University
Hangzhou, Zhejiang, China
22351378@zju.edu.cn

Haoye Dong
Zhejiang University
Hangzhou, Zhejiang, China
donghaoye@zju.edu.cn

Shichao Huang
Zhejiang University
Hangzhou, Zhejiang, China
huangshichao@zju.edu.cn

Xueyan Cai
Zhejiang University
Hangzhou, Zhejiang, China
caixueyan@zju.edu.cn

Kecheng Jin
Zhejiang University
Hangzhou, Zhejiang, China
jkcheng@zju.edu.cn

Fangtian Ying
MACAU University of Science and Technology
MACAU, China
group318@zju.edu.cn

Guanyun Wang†
Zhejiang University
Hangzhou, Zhejiang, China
guanyun@zju.edu.cn



**Figure 1: Examples of E-Joint Devices : a) Electronic Instrument; b) Posture Monitoring Chair; c) Modular Appliance Sets**

*The first two authors contributed equally to this work.
†Corresponding author.



*UIST '24, October 13–16, 2024, Pittsburgh, PA, USA*



ACM ISBN 979-8-4007-0628-8/24/10
https://doi.org/10.1145/3654777.3676398

## ABSTRACT

The advent of conductive thermoplastic filaments and multi-material 3D printing has made it feasible to create interactive 3D printed objects. Yet, challenges arise due to the volume constraints of desktop 3D printers and the high resistive characteristics of current conductive materials, making the fabrication of large-scale or highly conductive interactive objects can be daunting. We propose E-Joint, a novel fabrication pipeline for 3D printed objects utilizing mortise and tenon joint structures combined with a copper plating process. The segmented pieces and joint structures are customized in software along with integrated circuits. Then electroplate them for enhanced conductivity. We designed four distinct electrified joint structures in the experiment and evaluated the practical feasibility and effectiveness of fabricating pipes. By constructing three applications with those structures, we verified the usability of E-Joint in making large-scale interactive objects and showed the path to a more integrated future for manufacturing.

## CCS CONCEPTS

• **Human-centered computing → Interaction devices**.

## KEYWORDS

3D printed electronics; Parametric joint; conductive filament;

**ACM Reference Format:**

Xiaolong Li, Cheng Yao, Shang Shi, Shuyue Feng, Yujie Zhou, Haoye Dong, Shichao Huang, Xueyan Cai, Kecheng Jin, Fangtian Ying, and Guanyun Wang. 2024. E-Joint: Fabrication of Large-Scale Interactive Objects Assembled by 3D Printed Conductive Parts with Copper Plated Joints. In *The 37th Annual ACM Symposium on User Interface Software and Technology (UIST '24), October 13–16, 2024, Pittsburgh, PA, USA.* ACM, New York, NY, USA, 18 pages. https://doi.org/10.1145/3654777.3676398

## 1 INTRODUCTION

With the advancement of personal fabrication technologies such as desktop 3D printers and laser cutting, more common users can freely create physical objects of their design [52]. One area of the application that has received considerable attention is using 3D printing technology to create interactive objects [1, 2, 6, 9, 21]. This printing method enables 3D-printed objects with integrated circuits, providing opportunities for rapid prototyping and prototyping exploration in the HCI research field. Concurrently, as electronic products continue to grow in popularity, there is a rising demand for manufacturing large-scale interactive objects. However, for personal manufacturing in the HCI field, traditional manufacturing methods are limited by the size constraints of desktop 3D printers. This poses challenges when trying to manufacture interactive objects that exceed the printer's forming volume [34, 37, 50]. When products exceed these volume restrictions, connections between various components inevitably become an issue. Traditional methods for physical connections between parts include adhesive bonding [70], fasteners [23], and hot melt [15, 58]. These methods might be difficult to implement and could compromise the stability of the connected parts. For electrical connections, techniques such as welding [33], magnetic connection structures [13], connectors, and probe contacts [49] are typically employed. However, there are still relatively few methods for satisfying physically and electrically stable connections in the field of personal fabrication of interactive objects.

On the other hand, due to the constraints of the conductivity of existing printing materials, most existing applications are capacitive sensors [3, 16, 20, 26]. Selective electroplating of 3D interactive objects has attracted attention in the HCI field in recent years, offering new opportunities for manufacturing interactive objects with higher conductivity [37]. However, existing selective electroplating is usually limited to the outer surface of the object, leaving the circuits vulnerable to external factors. Under high-load conditions, high currents and heat generation in surface circuits can also pose safety threats to users [20]. Furthermore, existing solutions to the cross-line interference problem predominantly involve via holes, and most can only accommodate two layers: a front layer and a back layer [20, 61]. These problems limit the ability to manufacture more complex large-scale interactive objects.

To address these existential issues, we propose E-Joint, a design and manufacturing technique for building large-scale 3D printed products. The inspiration was taken from traditional Chinese mortise and tenon techniques, and we used improved circuit design to realize the interconnection between different components. These are designed with a connection structure that allows the parts to be connected by a simple assembly process, ensuring a stable contact of the conductive circuits. Further, to cater to different connection scenarios, we have designed four types of electrified joint connections (straight joint, dovetail joint, expansion joint, and spring-clip straight joint). Additionally, we have proposed a method for implementing high-load internal circuits, which can perform electroplating within large-scale 3D-printed interactive objects by establishing cavities within the object. This allows these 3D interactive objects to be embedded in high-load conductive circuits. In order to make our approach more accessible to users (researchers, designers, and artists in the HCI field who have a basic understanding of electrical knowledge and personal manufacturing experience) , we have developed an application extension based on Rhino3d, which includes built-in functions such as model segmentation, generation of electrified joint structures, and creation of internal three-dimensional circuits.

In the fabrication pipeline of E-Joint: (1) users utilize the Rhino plug-in we provide to lay out circuits and plug-in structures on their created models and then export them for 3D printing; (2) users electroplate the printed parts, causing the exposed conductive PLA parts to be copper-plated; (3) users embed the required electronic components into the machined 3D printed parts and assemble all the parts to complete the prototype production pipeline.

Subsequently, we conducted a series of evaluations on the joint structures and electroplated circuits to verify the reliability of the E-Joint. Finally, through three application cases (posture monitoring chair, electronic instrument, and modular appliance sets), we demonstrated large-scale interactive objects constructed using different forms of joints. We demonstrated that the E-Joint is a manufacturing method that can contribute to the construction of large-scale interactive objects.

In summary, the contributions of this paper are as follows:

1) A novel fabrication pipeline that focuses on electroplating enhanced electrified joints to create large-scale 3D printed interactive objects.

2) A software to separate and customize joints for large-scale 3D printed objects.

3) The evaluation of the electrified joints and the feasibility of the fabricated pipeline.

## 2 RELATED WORK

### 2.1 Fabrication of Interactive Prototypes

Historically, the field of HCI has been dedicated to integrating interactive interfaces with physical prototypes [63]. Researchers have continued to explore methods for building interactivity on physical surfaces, such as spraying conductive materials [13, 64, 71], flexible deformation [18, 31], screen printing [42, 43, 65], and inkjet printing [27, 67]. Many works attempt to lay out conductive materials on prototype surfaces to fabricate circuits [69] and embed electronic functions [68] that interact with each other. For example, SurfCuit [57] achieves interaction by embedding copper tape in V-shaped channels laid out on the surface of 3D printed objects and soldering electronic components. Narjes et al. [46] created Print-A-Sketch, which combines hand-drawing and functional electronic printing, supporting sketching interactive interfaces on everyday objects. These methods achieve interactive functions by attaching materials to complete prototypes' surfaces.

Other researchers have explored how to fully utilize the potential of objects to create electrical functionality while maintaining surface properties. They have also work to achieve designs based on highly curved organic geometries and varying visual-tactile surface properties. For example, Freddie et al. [20] described a thermoformable circuit board (TCB) technology that utilizes the thermoforming properties of 3D printed plastics, electroplating, and thermo-bending the 3D printed parts to construct good electrical performance. FiberWire [53] formd low-resistance conductors through laser ablation and fiber printing between layers of carbon fibre composites, realizing the design of carbon fiber-based circuits inside mechanically robust parts. ObjectSkin [17] added conformal interactive interfaces to everyday objects using hydrographic printing techniques, enriching the interaction possibilities of geometric objects. Gabriel et al. [48] used silver nanoparticle ink to print functional conductive patterns on 3D objects at unconventional angles, enabling circuits to hydro-print different 3D printed structures and materials at low temperatures.

### 2.2 Modular Design and Personal Fabrication

With the widespread adoption of rapid design and manufacturing, there is an expectation for individuals to engage in a variety of personal creations using personal fabrication tools. However, due to the volume limitations of personal fabrication tools, traditional fabrication methods have encountered difficulties in producing large-scale interactive products. Researchers have attempted to explore how to connect one component to another through a pair of matched joints and investigate the generation of binding forces between components, including the use of traditional joining methods such as adhesives [24, 56, 59], riveting [4, 25, 66], and welding [33, 36, 41].

In addition to these traditional methods, there are many researchers who try to deform materials [19, 60, 62] or attempt to create innovative assembly structures. For example, Kim et al. [29] designed a reconfigurable legged robot that utilizes a magnetic mechanical coupler to couple the legs to the body magnetically. BitSnaps [51] are color-coded magnetic connectors located at each end of all littleBits modules, allowing users to make their modules by connecting BitSnaps to the two lots of a printed circuit board. These tools all require new modules to be placed on top of existing parts to complete the connection between parts.

Other works have attempted to modify existing parts to create more integrated matching patterns. For example, FoolProofJoint [44] is a software tool that simplifies the assembly of laser-cut 3D models and reduces the risk of incorrect assembly by modifying finger joint patterns. MatchSticks [55] is a digital woodworking fabrication system that allows users to more efficiently express their design intent directly to CNC fabrication tools, creating different joints to join two separate pieces of wood. However, such methods rely on the reduction of available materials and require the use of large machining equipment. Oh, Snap! [49] proposes an interface concept that magnetically connects 3D objects to conventional electronic devices.

Meanwhile, researchers are exploring how 3D printing can be used to construct flexible and adaptable connection structures. TrussFab [35] is an integrated end-to-end system designed with a snap-and-thread connector to connect plastic bottles, allowing users to fabricate large structures that are robust enough to be used on desktop 3D printers. Koga et al. [32] proposed a new Ajax pin snap-in joint type based on fully 3D printed parts. Snap-in joints, and Ajax pins generate mechanical and bearing forces at the interface between parts to achieve joint strength comparable to adhesives and metal bolt joints. Song et al. [50] proposed a novel voxel-based approach that divides a 3D object model of a given general shape into interlocking 3D parts so that the 3D object can be printed together with smaller parts connected by 3D interlocks.

However, these designs only consider connections in terms of shape and structure. If it is desired to continue implementing electrical functions or installing electronic components between these parts, additional wiring connections, embedding of magnetic components or soldering may be required. This means more steps and longer manual handling times. Therefore, we are exploring a connection structure that can conveniently realize both physical contact and electrical function simultaneously.

### 2.3 Realization of the Conductive Function

Conductive materials play an essential role in scientific research and engineering applications. In the manufacturing industry, conductive materials and processes are often sought to meet the need to implement electronic functionality.

Conductive silicone has the advantages of good adhesion, wide strain range, low resistance and high sensitivity [38]. CurveBoards [72] provides a new electronic prototyping technique by filling channels with conductive silicone to form conductive circuits.

Conductive inks have excellent conductivity and flexibility, which are critical for constructing the next generation of flexible electronic devices [47]. It is typically used in combination with techniques such as inkjet printing [45, 67], spray painting [71], screen printing [42, 43, 65], and water transfer printing [48]. For example, Feng et al. [13] sprayed conductive silver ink onto laser-cut acrylic panels to

create a design and fabrication technique that combines electronic circuits and mechanical structures for interactive prototypes. Using screen printing technology, Kim et al. [28] fabricated a potentiometric sodium sensor based on a two-electrode structure with fast response time, high sensitivity, repeatability and selectivity.

Conductive liquid metals, featuring high conductivity and stretchability, have emerged as a promising solution for robust and durable electronics. For instance, Fassler et al. [12] encapsulated liquid alloys as a conductive medium in silicone, ensuring that the circuit components within the silicone retain their electronic functionality after stretching. These soft electronic devices can be placed around the skin and joints without interfering the body's natural compliance and movement. Cao et al. [11] explored the immense potential of conductive liquid metals in guiding the development of future epidermal devices and systems. Nagela et al. [39] proposed a scalable and achievable DIY fabrication method to fabricate silicon-based devices using silicone and conductive liquid metals. Liquid metals or their alloys offer superior alternatives to conductive and functional components for stretchable electronic products due to their high conductivity and excellent fluidity.

Conductive PLA is known for its high strength, flexibility, and abrasion resistance and has also been developed for use in environments with high thermal loads [8]. Brito et al. [10] deposited conductive materials on images to provide auditory feedback through printed components to assist visually impaired children in reading. [40] applied 3D printed conductive models to augmented reality (AR) environments, enabling bidirectional interaction between the physical world and the digital world. Flowers et al. [14] employed a bi-material fused filament fabrication technique to 3D print electronic components and circuits from conductive thermoplastic filaments, demonstrating the potential of 3D printing in creating complex 3D circuits consisting of embedded or entirely printed electronic components.

Copper, with its excellent electrical conductivity, thermal conductivity, corrosion resistance and low cost, is the preferred material for realizing electrical functions [22]. SurfCuit [57] soldered electrical components to interact with each other using a melting technique where highly conductive copper were firmly anchored to the surface of the 3D printed parts. Angel et al. [5] selectively electroplated copper onto printed parts to improve electrical properties and print more usable electromechanical systems. Kim et al. [30] demonstrated that one-step electrodeposition is a fast and straightforward way to enhance the conductivity and performance of 3D printed electronic components.

## 3 BASIS OF E-JOINT

This section describes a fabrication method that enables the 3D printing of large electronic products. In our approach, we use bi-material 3D printing to fabricate structures, form the electronic circuits using conductive PLA parts by copper deposition, and finally use the E-Joint to connect the different parts physically. We will describe in detail (1) how E-Joint enables object assembly and (2) the principle of circuit laying.

### 3.1 Create integrated connection structures between components

E-Joint has significant advantages as a method of joining components that differentiate it from fasteners, adhesives and welding: (1) it does not require additional joining components, reducing the total number of components and avoiding damage from the pressure brought by fasteners on segmented components; (2) it provides a faster method of installation compared to adhesives and hot melting; and (3) it achieves greater structural strength by locking the physical structure.

The E-Joint structure can be divided into mortise and tenon joint forms for mechanical connections and the circuit components for electrical connections. The electrified joint design is the core for connecting various components. It allows independent, loose components to be combined into load-bearing structures while completing the circuit connections between the members. Figure 2 shows an example of the integrated structure of the E-Joint. We utilize mortise and tenon joint structures to achieve the locking of the components, and we employ a one-piece moulding process to incorporate conductive traces within the mortises and tenons. During assembly, the electrical circuits are also connected to each other. In our example, component X and component Y are connected by insertion, resulting in the illumination of an LED light on component Y (Figure 2-b2).

### 3.2 Create highly conductive traces on the surface and inside of components

Low conductivity traces using multi-material printing. We used conductive PLA doped with 15% carbon nanotubes to construct low conductivity traces with a resistance of 120 Ω/cm on a 1.75 mm diameter filament. Unlike conventional methods of selective electroplating using conductive PLA, our method involves creating cavities around the conductive traces (Figure 2-c1), allowing the electroplating solution to enter the interior of the object and plating the conductive traces. In this way, our method supports the construction of 3D conductive circuits inside the objects.

Copper plating on the surface of the circuit. Electroplating requires additional equipment, including a DC power supply, a magnetic stirrer etc. but these equipment and materials are relatively accessible. By employing the electroplating process, we can convert the original high-resistance printed circuits into low-resistance, high-performance circuits, significantly broadening the application scenarios of our method. The electroplating process is described in detail in section 4.3. To facilitate users to hold parts of various shapes during the electroplating process, we set up a clamp plate on the outside of the circuits, which is also printed with conductive PLA. These software-generated clamp plates can be easily removed with pliers after electroplating (Figure 2-b1).

Create slots in the structures. Electronic components should also be embedded in these structures to form electronic circuits on the surface and inside the objects. We set up two types of slots: electronic surface mount slots (Figure 2-c3) and electronic pin slots (Figure 2-c4). Both types of slots are built on conductive PLA, so the surfaces in contact with each other will also be covered with electroplated copper, resulting in better connection performance [54].

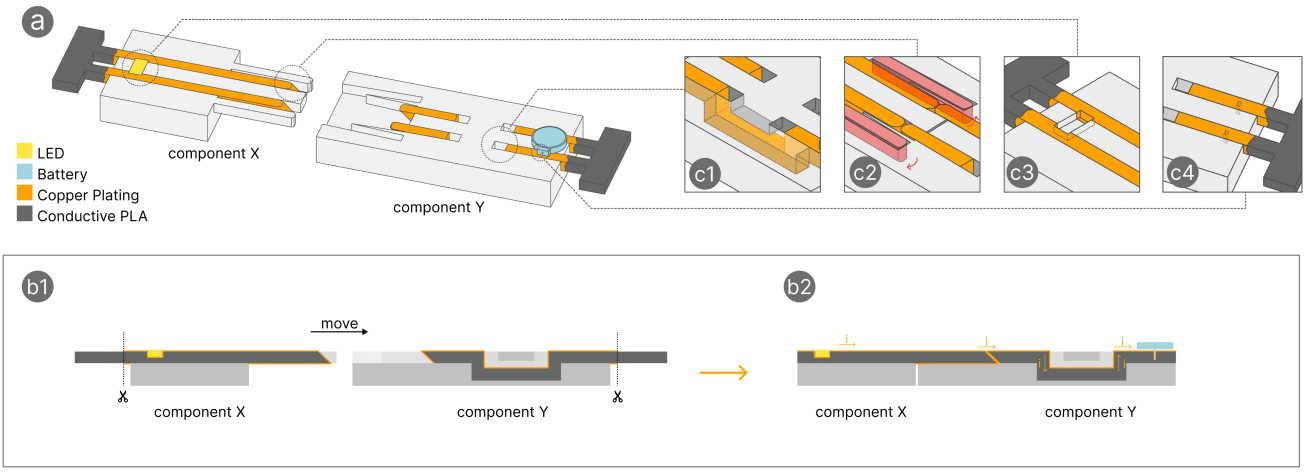


**Figure 2: a) An integrated instance of E-Joint; b) b1: The cross-sectional view before E-Joint assembly; b2: The cross-sectional view after E-Joint assembly and removal of clamping pieces; c) c1: The internal cavity structure; c2:Expansion tenon insertion process (the part where deformation bending occurs is marked in red); c3: The cavity for placing surface-mount devices; c4: The cavity for placing plug-in components**

## 4 FABRICATION PIPELINE

In order to provide details of the fabrication process for the target population of this paper, in this section we will introduce how E-Joint simultaneously achieves physical structure connections and electrical performance connections between different 3D printed parts to construct large-scale interactive objects that exceed the molding volume of the printer. We use the fabrication process of a novel electronic musical instrument as an example (Figure 3), showing the entire process from model creation to full presentation.

### 4.1 Model Design

Our software is built in Rhino3D and uses the parametric capabilities of Grasshopper to assist users in completing their designs (Figure 3a). It also leverages visual scripting extensions to facilitate more convenient operations for users. Designers first import a basic model of the circuit into the software environment, which has not yet been connected or split. Users are required to manually split the original model and place the parts that need to be closely connected. Subsequently, users select two blocks to be connected and use the auxiliary design tool to generate E-joints in the area where they meet. The auxiliary design tool helps users not only to create E-joints but also to adjust the various sizes and parameters. Moreover, establishing an appropriate gap between the E-joints is crucial, as it significantly determines the quality of the joint. The size of the gap should be determined by the printer used by the user. For the printer and parameter settings we use, tests have shown that setting the gap to 0.1mm (0.15mm for spring-clip straight joints) allows for a proper interference fit between the tenon and mortise. Additionally, our software environment provides an option to set the gap size, enabling users to match different devices. Designers can then define the layout and orientation of the circuit and decide whether the circuit will be on the surface or inside the object. If the designer places the circuit inside the object, the software generates a cavity for electroplating while creating the conductive trace, allowing the electroplating solution to enter the object and plate the internal surface of the circuit during the electroplating process. Finally, users have the option of generating clamp plates at appropriate locations for electrifying the conductive parts during the electroplating process. After completing the design, the software can export various components in STL file format for 3D printing.

### 4.2 3D Printing

Once the design is complete, users need to use multi-material printing to fabricate the parts (Figure 3b). In this work, we use the Bambu Lab X1 FDM 3D printer [7]. The machine has a molding size of 256mm × 256mm × 256mm using a 0.4mm hot melt nozzle and we use the Bambu Lab slicing software. For ordinary PLA filaments, we use the official white PLA Basic filaments from the Bambu Lab. The commercial conductive PLA we use (from Hangzhou Zhuoxin Universal Materials) is low in cost, easy to obtain, and has similar print parameters to ordinary PLA and can be used to print on a single extruder. The appropriate slicing setting should be noted. Previous studies have shown that there is a large resistance between conductive PLA layers. Therefore, using thicker layers not only facilitates rapid prototyping but also reduces the resistance of the printed parts in the z-axis direction. We use 100% internal filling, a linear filling method and more than 5 wall layers in the slicing software to ensure that the internal filling direction is the same as the wiring direction. These settings improve the conductivity of the circuit to a certain extent. When building printed parts with internally conductive circuits, it is recommended to use a method that only generates supports on the printing platform to avoid non-removable supports. For the extrusion settings, we set the extrusion temperature to 210℃. The print speed is set to 200mm/s to rapidly fabricate large-scale objects, and the temperature of the hotbed is kept constant at 50℃.

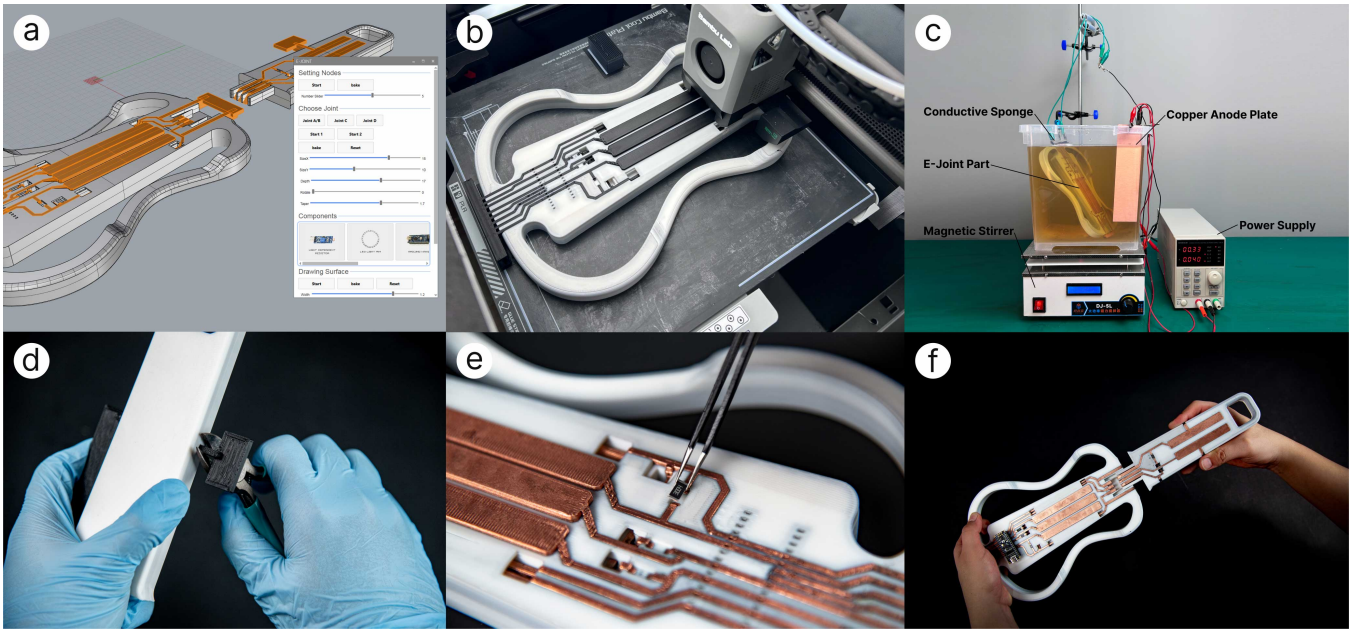


**Figure 3: Example of the E-Joint fabrication process: a) Laying out the lines on the model and arranging the joint structure using the E-Joint parametric design tool; b) Printing the model using nonconductive PLA and conductive PLA; c) Plating in the plating solution; d) Post-processing of the plated parts; e) Placement of electrical components; f) Assembly by insertion**

Additionally, to avoid cross-contamination between different types of filaments, a longer filament cleaning length should be set. In our experience, when using a wiping tower of 35 × 35mm or larger and a purge length of over 600mm, the conductivity of the conductive PLA filament is not affected.

## 4.3 Copper Electroplating

Once 3D printing is complete, the next step is to copper electroplate the printed parts. During the electroplating process, the conductive PLA material is used as the cathode, while the copper foil serves as the anode, and both electrodes are immersed in the copper electroplating solution. A direct current is then applied across the two electrodes, causing the current flows from the anode to the cathode. This results in the transfer of copper metal ions from the solution to the cathode of the conductive material of the printed object, resulting in the deposition of copper on the surface of the conductive material. The copper plating on conductive PLA surfaces can significantly enhance the conductivity of the object by five orders of magnitude. The electroplating solution for this project consists of copper sulfate, sodium hydroxide, complexing agents, brighteners and stabilizers. Among them, $CuSO_4 \cdot 5H_2O$ (160 g/L) provides the required copper ions for electroplating, NaOH (20 g/L) regulates the alkalinity of the electroplating solution and provides the necessary alkaline environment, EDTA (12 g/L) mainly acts as a complexing agent and plays a certain role as a promoter and stabilizer, and sodium benzenesulfonate $NaC_6H_4SO_3$(25 mg/L) acts as a brightener.

In the preparation, an appropriate amount of pure water is first put into the reaction tank, and $CuSO_4 \cdot 5H_2O$ is added and stirred evenly. Then add NaOH slowly, continuing to stir well. Next, add EDTA and continue stirring until completely dissolved. Finally, add $NaC_6H_4SO_3$ and stir well. Based on our experience with copper plating, we began with a constant current of 0.04 A at a room temperature of 25℃ until a visible thin copper layer was formed over the entire length of the circuit (about 1 hour). The current was then reduced to 0.02 A (about 4-7 hours). A magnetic stirrer was used at 400 rpm throughout the plating process to ensure uniform distribution. The power supply's positive terminal was connected to the copper sheet and the negative was attached to the component being plated. When connecting components with alligator clips, we cover the conductive sponge in the holding part to enhance the electrical connection.

## 4.4 Reprocess

After electroplating, the parts are rinsed to remove all electroplating solutions. The electroplated parts are then immersed in a passivation solution for 1 minute. It is recommended that a hairdryer is used to dry the electroplated surface. This is because if it is not dried quickly, the wet plating will react with the air to form copper oxide which will affect the quality of the electroplating. In actual operation, we use a hair dryer blowing back and forth at a temperature of 50℃ for 2 minutes to achieve complete surface drying. After air drying, we recommend that users spray transparent protective paint to protect the plating better. Finally, use a plastic nipper to cut off the connection clamp plate (Figure 3d) and use a file, sandpaper, or grinding wheel to smooth the trimmed part.

### 4.5 Assembling

After plating, the electronic components will be assembled into their corresponding positions using the plug-in method (Figure 3e). Finally, the user connects the parts according to the joint structure (Figure 3f). If the parts are too large during the joining process, a tool such as a rubber mallet can be used to strengthen the joint.

## 5 ELECTRIFIED JOINTS

To support other designers in using 3D printers to create large interactive objects, We electrically transformed four types of joint structures to enable them to complete the connection between interactive object components. This section introduces these electrified joint connection structures and their working and design principles. These connection structures can inspire users to create large electronic products based on their individual creativity.

These basic E-Joint structures comprise the straight joint, dovetail joint, expansion joint, and spring-clip straight joint (Figure 4). They can be adjusted to various sizes for connecting parts and support multi-line connections. For optimal structural stability, we suggest using a single mortise and tenon with a thickness of at least 20mm and a width of 50mm or more. Based on testing, a single conductive trace should be 3mm wide or more, with the space between two traces not less than 1mm for improved performance. In order to achieve optimal structural stability, we conducted specific dimensional standards, as illustrated in (Figure 5). (Figure 5a1) shows a top view of the assembly with conductive traces, (Figure 5a2) shows a sectional view along the a-a line, (Figure 5a3) shows a top view of the assembly without conductive traces, and (Figure 5a4) shows a sectional view along the a'-a' line, with subsequent figures following the same format. We recommend the use of a single mortise and tenon with a total thickness ($T_{\text{total}}$) of at least 20 mm and a total width ($W_{\text{total}}$) and length ($L_{\text{total}}$) of at least 50 mm. According to our tests, a single conductive trace should have a width ($X$) of at least 3 mm, and the thickness ($Y$) should be at least 4 mm. To enhance performance, the spacing ($\Delta X$) between two conductive traces should be no less than 1 mm. For example, the Expansion Joint, at its minimum structural width (50 mm), can support up to 4 circuits passing through at most. The dimensions of each characteristic electrical mortise and tenon joints are detailed in the corresponding subsection of Section 5.

In our print setup, the tolerance size for the three types of mortise and tenon joints is 0.1mm before assembly. By designing the splicing with this data, a strong physical connection can be achieved, preventing repetitive assembly of a, b, c. For d, a tolerance size of 0.15mm allows for a stable connection that can be disassembled without damage, enduring repeated insertion and removal operations.

The E-Joint is parametrically generated using the auxiliary design tool. Selecting from one of the four types of electronic tenon-and-mortise joints based on the requirements, our tool is then capable of generating the E-Joint at the specified location. The tool automatically performs Boolean operations on adjacent entities, contingent upon the positive or negative values of the depth measurements. The dimensions, position, number of lines, and mating tolerance of the E-Joint can be set by the user. The auxiliary design tool and the design process will be described in detail in Section 6.

### 5.1 Straight Joint

The most straightforward E-Joint mechanism is based on an electrified modification of the straight joint, as shown in Figure 4a with a tenon at one end and a joint eye at the other, connected by an inserted interference fit. To ensure that the wiring can be maintained when the parts are mated, the software generates a protrusion on the conductive trace side of the joint eye of 0.3mm, this value is obtained through an iterative test. Additional dimensions are illustrated in (Figure 5a), where $L_1$ is recommended to have a uniform thickness, typically equivalent to $T_{\text{total}}$, and $W_1$ is suggested to be twice the value of $T_{\text{total}}$. The tenon and mortise's size and depth determine the connection's power. E-Joint's software environment provides these setup options, allowing for three-dimensional circuit construction that shifts the circuit layout from one spatial plane to another.

### 5.2 Dovetail Joint

The dovetail joint has a high tensile strength. This connection structure allows components easily assembled from one direction (Figure 4b) while maintaining a stable lock structure along its axis. For different application scenarios, For various application scenarios, the angle of the dovetail tenon, denoted as $\theta_1$, should be greater than $45^\circ$ and less than $80^\circ$, as depicted in (Figure 5b). The length of $L_2$ should exceed 12 mm. And users can decide the required pitch in the software. Similar to the straight joint setting, the part of the circuit contact will also generate corresponding protrusions to ensure the stability of the circuit contact.

### 5.3 Expansion Joint

In this connection structure, two auxiliary tenons are added on both sides of the central tenon for locking (Figure 4c). After insertion, the auxiliary tenons on the left and right sides will slide inward and deform under the guidance of the wedge-shaped tenon slot, bringing extra expansion pressure to the connection structure (Figure 2-c2). Meanwhile, the sloped setting at the end of the circuit will generate a reaction force caused by the deformation pressure, ensuring that the contact surface maintains a stable connection. The specific dimensions are illustrated in (Figure 5c). The total width of the circuit area is given by the formula $nX + (n-1)\Delta X$, where, based on our experience, the Expansion Joint can support up to 4 circuits at a minimum structural width of 50 mm. The angle $\theta_1$ should be greater than $60^\circ$ and less than $80^\circ$. The length $L_3$ should exceed 22 mm, and $\theta_3$ should be greater than $30^\circ$ and less than $60^\circ$ to achieve more stable performance.

Moreover, this contact surface with an elastic deformation structure can also bring a higher tolerance rate under the condition of multiple circuit connections, preventing the situation where some circuits are disconnected due to tilting the circuit contact surface under pressure. Therefore, this type of joint is suitable for situations that require multiple circuit connections, and users can set the number of circuits to be connected in the software environment.

### 5.4 Spring-clip Straight Joint

To achieve replaceable E-joint components, we designed a joint structure with a spring sheet (Figure 4d). The spring sheet structure

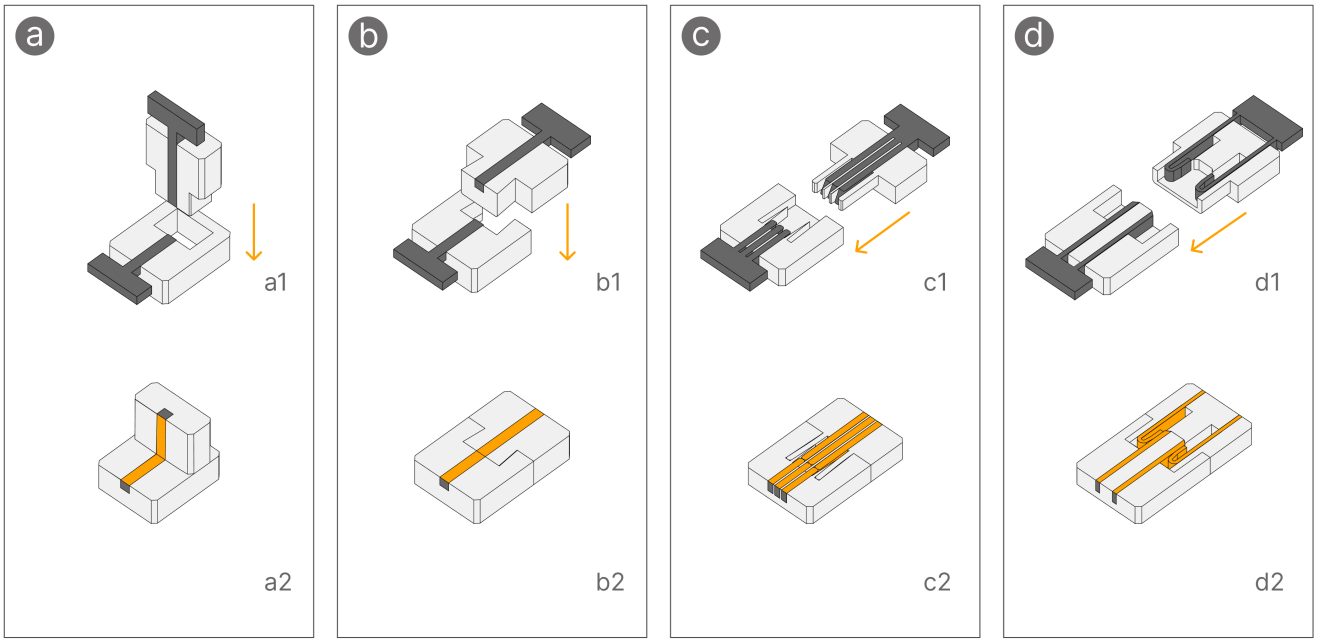


**Figure 4: Illustrates four types of electrified joint structures: a) a1: Straight joint; a2: Straight joint after electroplating and connection; b) b1: Dovetail joint; b2: Dovetail joint after electroplating and connection; c) c1: Expansion joint; c2: Expansion joint after electroplating and connection; d) d1: Spring-clip straight joint; d2: Spring-clip straight joint after electroplating and connection**

provides the friction force for component connection and undertakes the conduction function between components. Moreover, the more extensive elastic system can maintain a minor deformation during insertion, keeping the plating stable to withstand repeated plugging and unplugging operations. Specific dimensions are illustrated in (Figure 5d). The $L_4$ length controls the effective connection area and should be greater than 18 mm.

# 6 E-JOINT DESIGN EDITOR

## 6.1 Generate Grid Points

Users first import the original model into the Rhino3D software environment. Subsequently, users are required to manually segment the model at the expected locations, dividing the original model into separate but tightly abutting entities. By selecting the two entities that need to form a mortise and tenon joint through the panel, Grasshopper will generate selectable grid points where the two entities are in contact (Figure 6a). We referenced the TCB [20] for this feature. Users can adjust the spacing of the grid points according to their precision requirements, which facilitates better positioning and layout of the mortise and tenon joints. This precision determines the accuracy of the subsequently drawn circuit traces and the accuracy of the positions where the mortise and tenon structures are generated.

## 6.2 Generating E-Joints

After setting the spacing, users can choose grid points to determine the location of the E-Joints (Figure 6b). Depending on the connection requirements, users can select one of four types of E-Joints. The software then generates the corresponding E-Joint at the specified location. Based on the positive or negative value of the depth, the software automatically performs boolean operations of union or difference on the adjacent entities. Users can adjust the dimensions of the mortise and tenon structure according to their specific needs.

For the straight joint and dovetail joint, the mortises can be altered by adjusting the taper and setting the tilt angle to achieve the desired transition (Figure 6c). The expansion joint and spring-clip straight joint are developed based on the straight joint. They utilize the Box Morph component for mapping, which allows for the insertion of various mortise and tenon types. The size, dimensions, and angles of these joints are adjustable to fit the user's requirements.

## 6.3 Electronic Component placement

Users can select electronic components from the software's model library and place them on the grid points of the model. The software will automatically trim the original model to create grooves.

## 6.4 Generate 3D Conductive PLA Traces

One of the key features of the E-Joint Design Editor is that it allows users to construct three-dimensional circuit structures in space. Initially, users generate conductive traces on the surface by clicking on grid points. Once selected, the software automatically creates

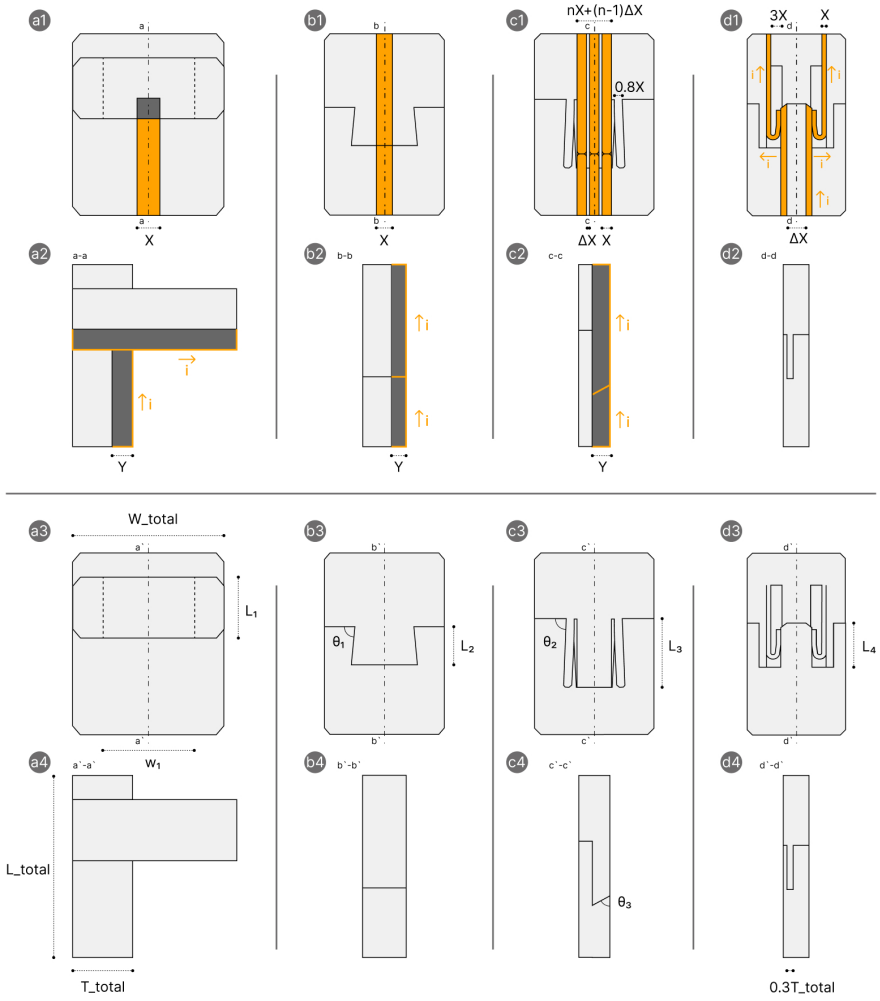


**Figure 5: The four types of electrified joint structures, dimensions, and current: a) a1: Top view of the straight joint after electroplating; a2: Sectional view along the a-a line; a3: Top view of the straight joint; a4: Sectional view along the a'-a' line. b) b1: Top view of the dovetail joint after electroplating; b2: Sectional view along the b-b line; b3: Top view of the dovetail joint; b4: Sectional view along the b'-b' line. c) c1: Top view of the expansion joint after electroplating; c2: Sectional view along the c-c line; c3: Top view of the expansion joint; c4: Sectional view along the c'-c' line. d) d1: Top view of the spring-clip straight joint after electroplating; d2: Sectional view along the d-d line; d3: Top view of the spring-clip straight joint; d4: Sectional view along the d'-d' line**

the trace and trims the original model (Figure 6d). Then, users can select the grid points on the conductive traces and adjust their positions on the z-axis to offset within the model, thereby constructing internal conductive traces. The software will automatically trim the original model to form an internal cavity that matches the internal conductive traces. Users can choose electronic components from the software model library to place on the model, and the software will trim the original model to generate slots accordingly. Users click on the end of the conductive trace and click the "Generate Clamp Plate" button, and the software will generate a clamp plate outside the original model (Figure 6e). In the software, the user can set the width and height of the conductive traces, the cross-sectional dimensions of the internal cavity, and the size of the clamp plates.

## 6.5 Exporting Printable Models

After the design is complete, users can export the designed model parts as STP format 3D files via the "Export File" option. The conductive traces and the original models are placed on different color layers, allowing users to make different slicing settings in the slicing software (Figure 6f).

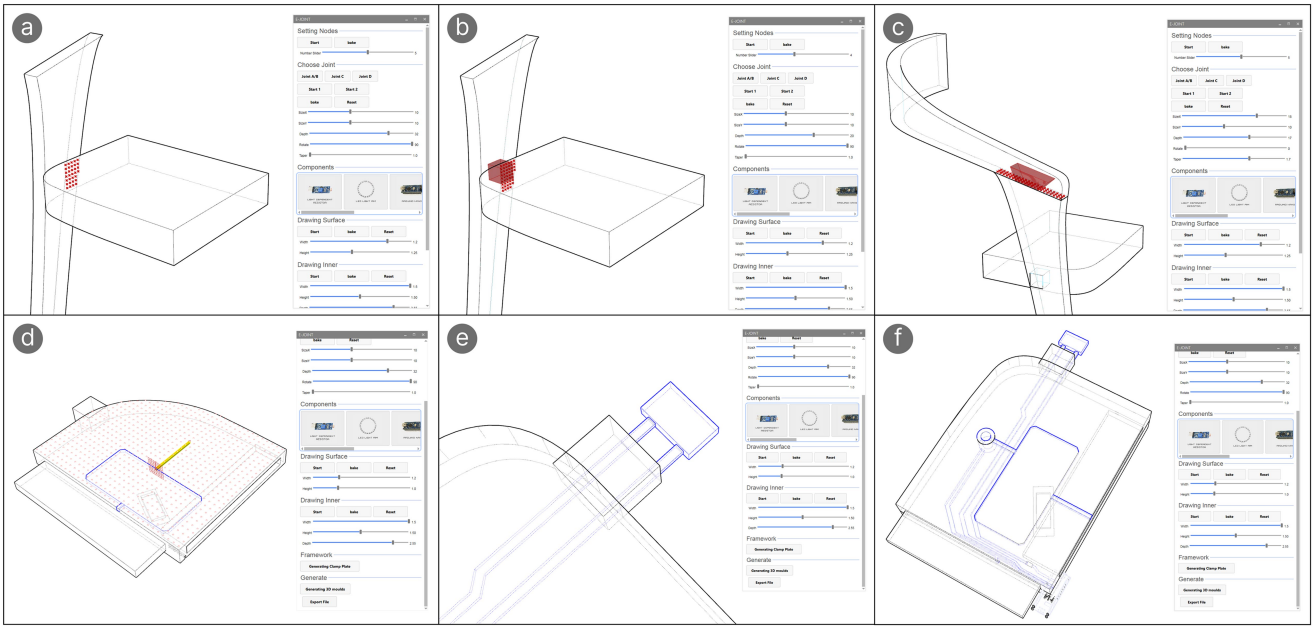


**Figure 6: The process of modeling with E-Joint: a) Select two objects and generate selectable mesh points at the fit; b) Generate straight joint mortise and tenon joint and boolean model; c) Generate dovetail joint mortise and tenon joint and boolean model; d) Generate selectable mesh points on the surface of the objects, select components from the library and place them to draw the conductive trajectory; e) Generating Clamp Plate; f) Generate a model of the component layer and export it**

## 7 EVALUATION

To determine the technical parameters of the pipeline, we deployed evaluations as references for choosing the specific parameters of the conductive PLA trace and the connection structure (Table1). Additionally, to prove the practical feasibility of our production traces, we conducted empirical evaluations of E-Joint's performance, including the quality of the connection and the stability of the joint structure's physical connection. All these evaluations were carried out using the same materials and methods as in Section 4.

### 7.1 Evaluation of Plating Circuits

*7.1.1 Line Width of Conductive PLA Traces.* When designing parameters for the circuit part, we first confirmed the minimum 3D printing width of the conductive PLA trace. We created a test piece with different conductive PLA trace widths, all with a line depth of 3mm. The conductive PLA line widths on the test piece range from 0.4mm to 6.0mm, each trace is 0.4mm wider than the previous one, and all trace lengths are 100mm. We electroplated the test piece with a constant current of 0.04A in an electrolyte solution for 10 hours. After electroplating, using high-precision resistance measuring equipment for four-probe measurement (Figure 7a), we found traces with a width of 2.0mm or more obtained good conductivity (resistance stable at less than 0.1 Ω for 100mm) (Figure 8).

*7.1.2 Cross-sectional Area of Conductive PLA Traces.* We designed a test piece with different cross-sectional areas to explore more reasonable conductive PLA trace layout parameters. The cross-section of the conductive PLA trace on this test piece is all square, with side lengths from 0.4mm to 3mm; each trace cross-section side length is 0.1mm longer than the previous one, and all trace lengths are 100mm. We also used a constant current of 0.04A and an electroplating time of 10 hours. After testing, traces with a cross-sectional area greater than 2.89mm² achieved good conductivity (resistance less than 0.1 Ω for 100mm) (Figure 9). As the cross-sectional area increased, the resistance gradually decreased, so we suggest that users choose a larger cross-sectional area as much as possible when establishing longer conductive PLA traces.

*7.1.3 Length of Conductive PLA Traces.* We conducted a continuous electroplating test for 10 hours on a conductive PLA trace with a cross-sectional area of 15mm² using a constant current of 0.04A. After the trial, we obtained a copper electroplated trace length of approximately 450mm (Figure 7c). The electroplated length is almost twice the width of our printer's moulding dimensions, meeting our needs in the prototyping process.

*7.1.4 Slope of Conductive PLA Traces.* We designed a test piece with different sink slopes to evaluate what kind of sink slope should be chosen when arranging circuits across the z-axis. The conductive PLA traces of this test piece had a square cross-section with a side length of 3mm. Each trace is sunk at a different angle by 10mm (Figure 7d). The test piece was electroplated with a constant current of 0.04A for 10 hours. The results showed that traces close to 90° have better conductive performance, and their occupation of the xy plane space is also the smallest, which is conducive to constructing complex multi-layer circuits. Therefore, we unanimously chose 90° as the slope when making space turns.

**Table 1: Evaluation Summary**

| Evaluation | Task | Goal |
|---|---|---|
| Minimum print line width circuit resolution, conductivity and parameter settings | Test the minimum line width that can be printed and plated | Evaluate the minimum line accuracy that can be supported on a plane during manufacturing |
| | Test the minimum conductive trace cross-sectional area that can be printed and plated | Evaluate the minimum line cross-sectional area that can be supported when size is limited during manufacturing |
| | Test the maximum achievable trace length | Evaluate the constraints on circuit length within a single component during manufacturing |
| | Test the angle of twist for the lowest trace resistance | Find the circuit transition angle that is most suitable for application to the manufacturing process |
| | The minimum cavity cross-sectional area that the test method can support | Tests the smallest cavity cross-sectional area that can be used in the manufacturing process |
| Electrical and mechanical connection capability of E-Joint | Test the electrical conductivity of four kinds of mortise and tenon joints | Test the electrical connection performance of the E-Joint to evaluate the applications it can support |
| | Test the maximum tension/shear forces that four mortise and tenon joints can support before structural failure | Test the mechanical connection properties of the E-Joint to evaluate the applications it can support |
| Stability of E-Joint pipeline | Test its yield in the case of repeated manufacturing | Evaluate the reliability of the workflow |

**Table 2: Stress test results of different joint configurations**

| Joint | Tensile Force(N) | | Frontal Shear Force(N) | | Lateral Shear Force(N) | |
|---|---|---|---|---|---|---|
| | M | SD | M | SD | M | SD |
| **Straight Joint** | 189.00 | 7.23 | 714.17 | 6.96 | - | - |
| **Dovetail Joint** | 429.50 | 7.85 | 135.33 | 7.27 | 593.67 | 3.16 |
| **Expansion Joint** | 253.83 | 5.70 | 78.83 | 5.49 | 528.17 | 4.88 |
| **Spring-clip Straight Joint** | 12.33 | 2.29 | 52.33 | 4.75 | 506.80 | 5.71 |

*7.1.5 Internal Cavity Size.* To investigate the relationship between the plating effect of internal circuits and the size of the cavity, we designed a test piece with different cavity cross-sectional areas. In this test piece, the cavities are all square in cross-section. The cross-sectional square side length increases from 3mm to 5mm, and the side length of each cavity section increases by 0.2mm from left to right (Figure 10a). We continuously electroplated this test piece for 10 hours with a constant current of 0.04A. After the process, each trace within the cavities had good electroplating. We used the four-probe method to measure the resistance of each trace (Figure 10b). The results show that the cross-sectional area of the cavity is positively correlated with the plating quality.

*7.1.6 Circuit Load Capacity.* E-Joint is a manufacturing method for large-scale 3D interactive objects with high conductivity. We have explored its load-bearing capacity to provide recommendations for circuit load. We used a direct current regulated power supply that can provide high current to load test copper-plated traces of different line widths. We continuously increased the voltage at both ends of the electroplated trace until the trace was burnt and failed (Figure 11a). Based on the results, we plotted a graph of the voltage-current relationship (Figure 11b) and the instantaneous load power of conductive PLA trace lines of different widths (Figure 11c). The instantaneous load of the 5.2mm line width conductive PLA trace can reach up to 58.625W, and its maximum current tolerance before burning out is 23.45A.

## 7.2 Mechanical Strength of Joints

In order to explore the physical connection ability of E-joints, we used four uniformly sized force test pieces to test the mechanical properties. The cross-section of the test pieces for each of the four different mortises was a square with a side length of 30 mm. We used a dynamometer and weights of different weights to perform tensile and shear force tests on the test pieces to observe their force-bearing capabilities under different working conditions (Figure 7b).

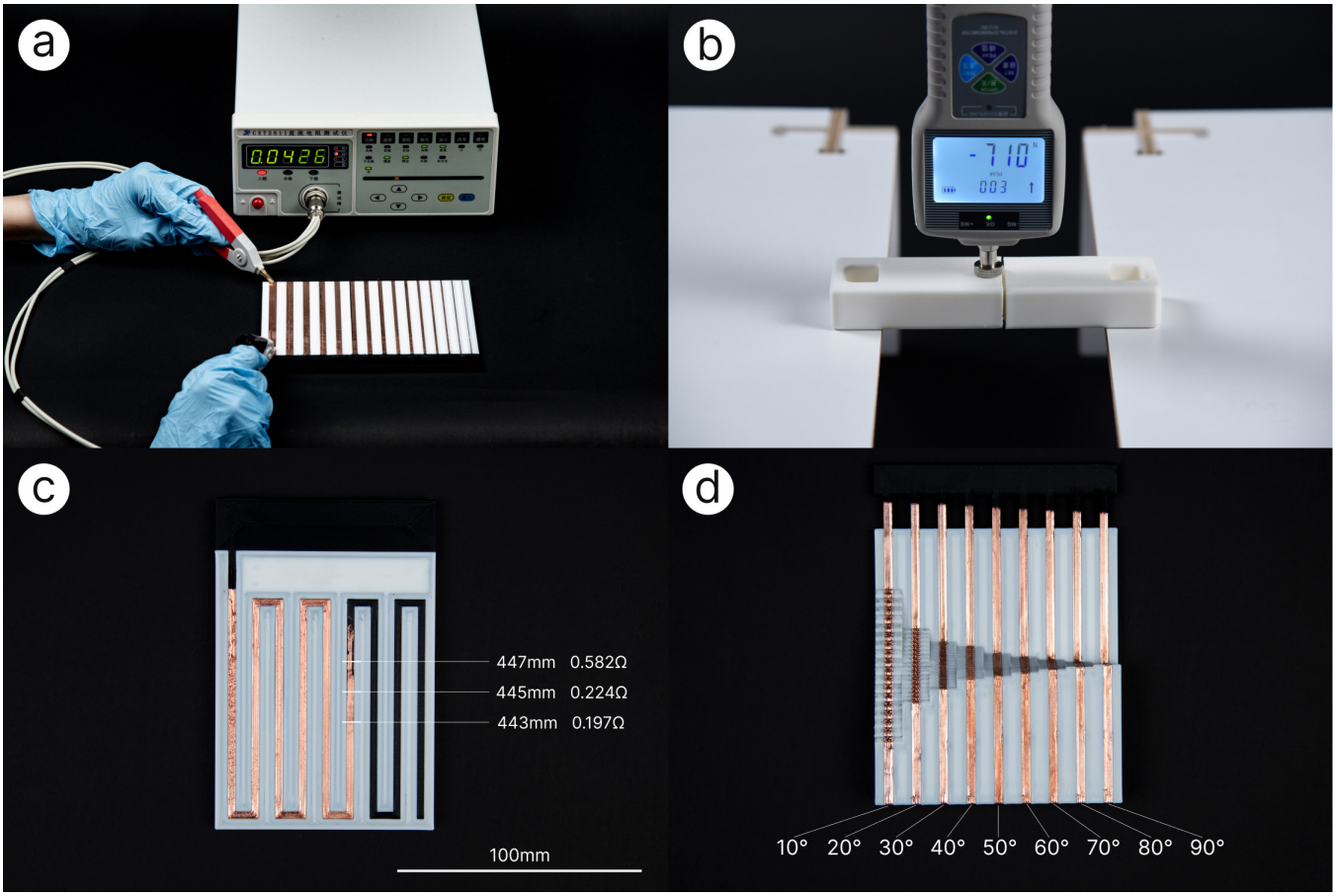


**Figure 7: a) Measurement of the resistance of the conductive trace using the four-probe method; b) Mechanical properties testing of the E-Joint; c) Results of the plating length test; d) Slope test pieces**

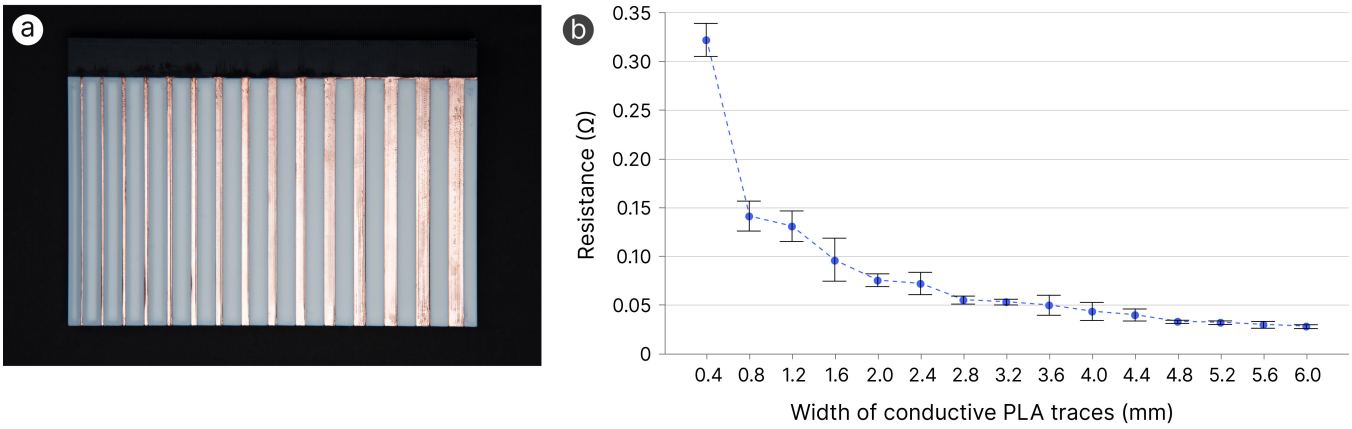


**Figure 8: a) Top view of test piece with conductive trace width; b) Resistance test results for different widths of conductive traces**

In the experiment, we continuously increased the pressure applied to the test pieces until there were obvious gaps at the connections. The test results are shown in the Table 2. For straight joint and dovetail joint that need to be connected with high strength, they both have strong shear resistance. For the expansion joint that needs to conduct multi-line connections, it has strong tensile resistance.

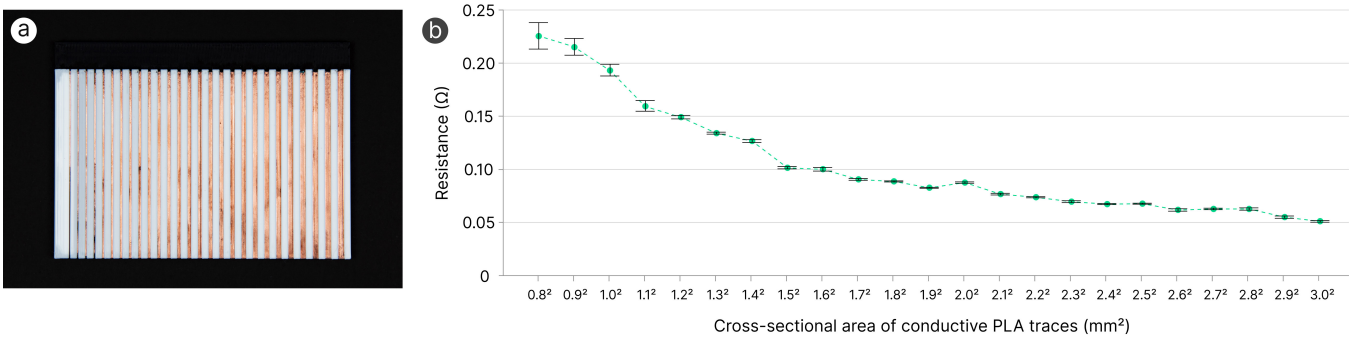


**Figure 9: a) Conductive PLA cross-sectional area test piece; b) Resistance test results of conductive PLA coatings with different cross-sectional areas**

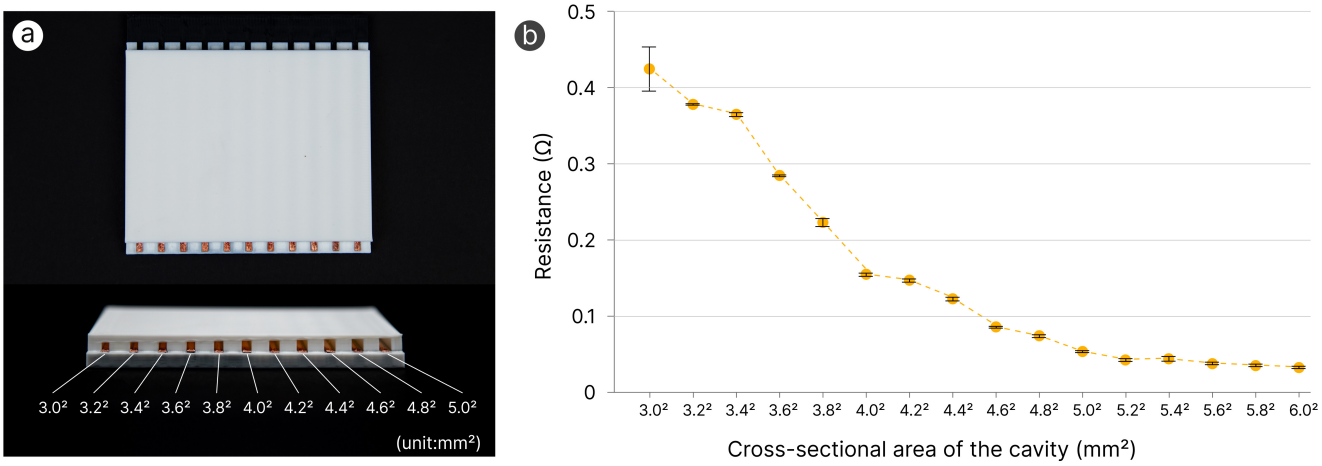


**Figure 10: a) Cavity cross-sectional area test piece; b) Resistance test results for different cavity cross-sectional areas**

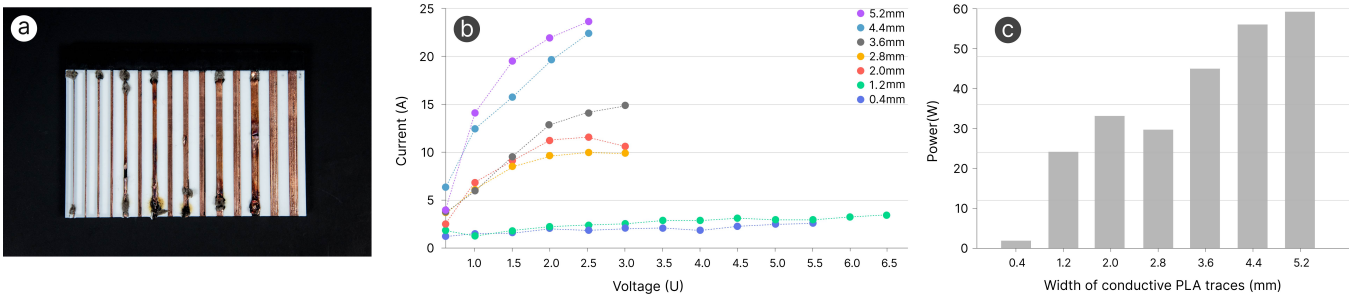


**Figure 11: a) line-loaded test pieces; b) line-loaded test results; c) maximum instantaneous power measured for different line-width coatings**

The spring-clip straight joint specifically designed for repeated insertion and removal, it can be pulled out with only a small force, making it easier for users to replace parts.

## 7.3 E-Joint connection evaluation

To evaluate the quality of the E-Joint connections, we manufactured 10 pairs of each type of joint structure to test the success rate of the connections. We also tested the resistance at both ends of the joint structure after connection. The test results are shown in the following Table 3. The results show that the E-Joint has good

**Table 3: Summary of the average value, standard deviation and range (maximal delta from mean) for the current of four joints structure after connection**

| Joint | M(Ω) | SD(Ω) | RangeΔ |
|---|---|---|---|
| Straight Joint | 0.0619 | 0.0160 | [-0.0196, +0.0253] |
| Dovetail Joint | 0.0636 | 0.0122 | [-0.0203, +0.0216] |
| Expansion Joint | 0.0437 | 0.0077 | [-0.0094, +0.0151] |
| Spring-clip Straight Joint | 0.0457 | 0.0074 | [-0.0151, +0.0102] |

connection performance and has good stability and consistency in repeated structures. In addition, for the spring-clip straight joint that needs to be inserted and removed repeatedly, we also conducted an endurance test of 800 insertions and removals, and it was still able to maintain good circuit connection ability (resistance less than 0.1 Ω) after the test.

## 8 APPLICATIONS

In this section, we will detail three interaction application instances to demonstrate the wide applicability of E-Joint to various types of interactive applications. They collectively incorporate all the mortise and joint connection structures and circuit deployment methods we have proposed, showcasing the capabilities of E-Joint in terms of connecting components, interaction mechanisms, and electronics.

### 8.1 Posture Monitoring Chair

E-Joint can construct large-scale interactive objects. We designed a posture monitoring chair assembled from 20 different parts, with final dimensions of 455mm × 424mm × 730mm (Figure 12). Such a large-scale 3D printed interactive object is rare, and the volume of this application is eight times the forming volume of the desktop printer we used. The posture monitoring chair connects the components with straight joints and dovetail joints. It can monitor the user's sitting posture through eight capacitive sensors set at different positions (Figure 12c). When the user's posture is incorrect, or they have been sitting for a long time, the chair leg flashes to alert the user (Figure 12d).

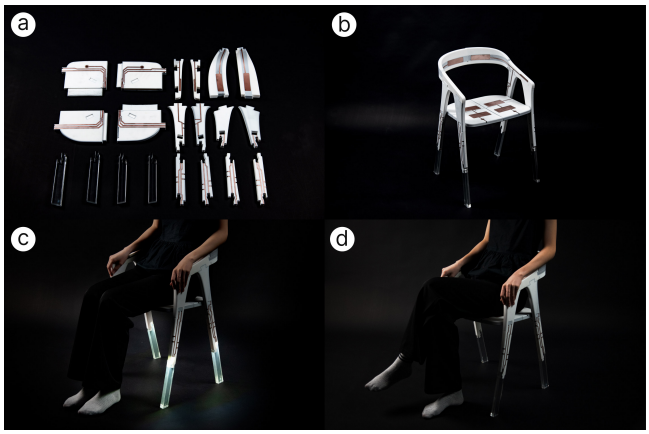


**Figure 12: Posture Monitoring Chair: a) Parts of the Posture Monitoring Chair before assembly; b) Form of the posture monitoring chair after assembly; c) Lights of the chair are always on when the sitting posture is correct; d) Lights of the chair go into blinking state to remind the user when the sitting posture is wrong**

### 8.2 Electronic Instrument

E-Joint can lay circuits inside objects and achieve multiple circuit connections. In this example, we designed a fusion electronic musical instrument of a ukulele and a violin using the mortise and joint connection structure, cavity circuits, and surface circuits (Figure 13). This is a personalized and novel instrument comprising a fingerboard area and a body area connected by insertion. Using expansion joints provides better lateral contact and improves longitudinal force resistance. We sank the circuits parallel to the touch area into the cavity to avoid interference between exposed circuits and touch areas. The electronic instrument has an Arduino expansion board, a buzzer, and three surface-mount resistors.

This electronic instrument provides two ways of use - you can play it like a ukulele by directly pressing the body sensing area (Figure 13c) with your fingers, and it will produce the sound of a ukulele. Alternatively, you can play it like a violin by using a bow

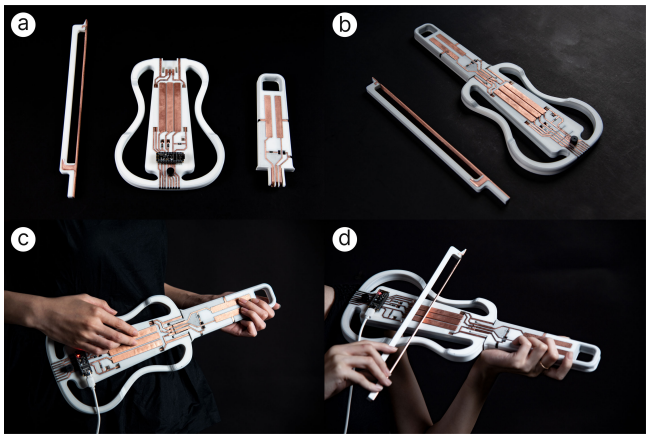


**Figure 13: Electronic Instrument: a) Parts of the Electronic Instrument before assembly; b) Completed assembled Electronic Instrument; c) Playing with fingers to produce ukulele sound color; d) Playing with bow to produce violin sound color**

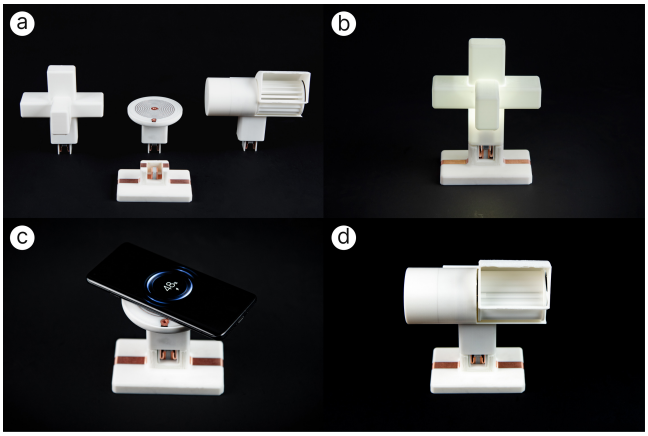


**Figure 14: Modular Appliance Sets: a) Parts of the Modular Appliance Sets before assembly; b) The Kong Ming Lock light illuminates when inserted into the base; c) The wireless charging pad powers the cell phone; and d) The desktop fan is in operation**

to touch the body sensing area (Figure 13d), and it will produce the sound of a violin. Different tones are made based on the touch location and bow position, and the fingerboard part controls the scale through the touch area.

### 8.3 Modular Appliance Sets

E-Joint is stable in connection and easy to insert and remove the required components. We used a spring-clip straight joint to connect the base to three appliances (Figure 14). The base is used to power the different appliances. Through simple insert and remove operations, users can switch between a desk lamp (Figure 14b), a desktop fan (Figure 14c), and a wireless charging base (Figure 14d). When inserted, the circuits on both sides of the spring-clip straight joints are connected, and power is supplied to the appliance. Due to the high conductivity of E-Joint, it is not limited to typical low-current applications such as sensors. It can bring more practical interactive objects to users, such as the fan and wireless charging base we showed, which can be used to charge smartphones and other devices.

## 9 DISCUSSION, LIMITATION AND FUTURE WORK

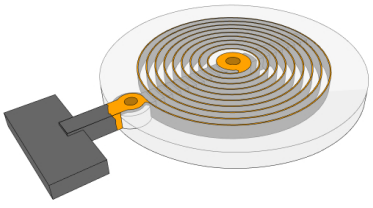

**Figure 15: Internal structure of the wireless charging pad: its conductive traces are connected in parallel inside**

Although E-Joint can connect both traditional and 3D printed objects, and possesses the capability to create large-scale interactive objects, it currently confronts several constraints that must be considered in the manufacturing process. In the following, we discuss these limitations and look forward to the future potential of 3D printed interactive objects.

### 9.1 Integrated Connection

In this paper, we present E-Joint's capability to achieve both physical and electronic connections simultaneously. However, due to the mechanical property limitations of PLA printing material, we found that deformation at the connection site can easily occur when connecting long rod-shaped objects (such as the legs of a chair in our case study application). This is due to the longer force arm applied externally, and the relatively smaller structure used for connection, and this deformation will accumulate when multiple sections are connected. Although E-Joint can still maintain normal connections in our case, the risk of connection failure increases when more joint structures are connected in series. In the future, we will seek better joint structures, try stronger printing materials such as carbon fiber reinforced PLA, and add settings in the software to remind users to set reasonable joint and mortise sizes under different structures to achieve higher success rates.

Secondly, the size of circuit connections can limit the scale and complexity of the objects that can be produced by our method, both in terms of mechanical strength and the number of circuits. Although larger-scale products generally imply a larger cross-sectional area at the joints, the issues of mechanical strength and the number of circuits can be overcome by simply increasing size and paralleling multiple E-Joints. However, it is still necessary to further evaluate the relationship between size and the number of circuits that can be handled. On the other hand, the current circuit layout is to place the circuits flat on a single layer, and in the future attempts will be made to place more circuits on both the top and bottom layers to increase the number of circuits that can pass through.

### 9.2 Copper Plating Traces

As mentioned in Section 6, although the conductive traces we use have a lower price and similar printing parameters to non-conductive PLA, which is conducive to rapid printing, their resistance is high. When it is necessary to electroplate a circuit with a smaller cross-sectional area and a longer distance, the problem of long electroplating time or difficulty in electroplating may occur. However, in Application 3, our wireless charging board module achieves rapid electroplating of the entire conductive PLA traces by paralleling them together (Figure 15). In addition, our method proposes a way to construct high-performance stereo circuits inside objects. We have conducted corresponding evaluations, but it does not cover many complex scenarios. In the future, we will carry out more evaluations to test its capability under more complex internal traces.

### 9.3 Large-Scale Interactable Objects

In our applications, the posture monitoring chair is the largest interactive object, demonstrating the ability to manufacture products far beyond its molding volume using a desktop-grade printer.

Compared with traditional manufacturing processes, our E-Joint application uses less manual labor time. However, for larger interactive products such as vehicles or even buildings, the printing speed and the cost of materials may become limiting factors. In future work, we will make modular improvements to E-Joint and attempt to construct larger interactive objects. We will try to combine E-Joint with traditional materials, using traditional materials in non-connecting parts, which will greatly reduce unnecessary printing time.

## 10 CONCLUSION

E-Joint is an innovative fabrication pipeline that, by applying joint structure principles and circuit connection structures, overcomes the limitations of traditional fabrication methods to achieve segmented fabrication of large-scale 3D printed products. This method is simple and efficient, able to solve the connection difficulties caused about by the volume limitations of desktop-level 3D printers and the high resistance characteristics of conductive print materials. Through electroplating technology, E-Joint can also achieve high-current applications on the surface and inside of objects, improving the reliability and functionality of electrical functions. We have also proposed four different electrified joint connection structures, and through examples, we have verified E-Joint's ability to manufacture larger and more usable interactive objects.

E-Joint's innovative solutions bring new possibilities for the manufacture of large-scale interactive prototypes using 3D printers, and also bring important technological advances to the 3D printing industry. With the further development and optimization of this method, we expect to see the creation of more complex and multifunctional 3D printed products that will drive innovation and development in this field. The emergence of E-Joint will promote further intelligence and personalization in individual manufacturing, bringing more convenience and possibilities to our lives and work.

## ACKNOWLEDGMENTS

This research was supported by the Fundamental Research Funds for the Central Universities (Grant No. 226-2024-00164), "Leading Goose" R&D Program of Zhejiang (Project No.2023C01216), Zhejiang Provincial Natural Science Foundation of China under Grant No. LR24F020001, Research Center of Computer Aided Product Innovation Design, Ministry of Education.

## REFERENCES

[1] Muhammad Abdullah, Romeo Sommerfeld, Laurenz Seidel, Jonas Noack, Ran Zhang, Thijs Roumen, and Patrick Baudisch. 2021. Roadkill: Nesting Laser-Cut Objects for Fast Assembly. In *The 34th Annual ACM Symposium on User Interface Software and Technology* (Virtual Event, USA) *(UIST '21)*. Association for Computing Machinery, New York, NY, USA, 972–984. https://doi.org/10.1145/3472749.3474799

[2] Harshit Agrawal, Udayan Umapathi, Robert Kovacs, Johannes Frohnhofen, Hsiang-Ting Chen, Stefanie Mueller, and Patrick Baudisch. 2015. Protopiper: Physically Sketching Room-Sized Objects at Actual Scale. In *Proceedings of the 28th Annual ACM Symposium on User Interface Software & Technology* (Charlotte, NC, USA) *(UIST '15)*. Association for Computing Machinery, New York, NY, USA, 427–436. https://doi.org/10.1145/2807442.2807505

[3] Marwa Alalawi, Noah Pacik-Nelson, Junyi Zhu, Ben Greenspan, Andrew Doan, Brandon M Wong, Benjamin Owen-Block, Shanti Kaylene Mickens, Wilhelm Jacobus Schoeman, Michael Wessely, Andreea Danielescu, and Stefanie Mueller. 2023. MechSense: A Design and Fabrication Pipeline for Integrating Rotary Encoders into 3D Printed Mechanisms. In *Proceedings of the 2023 CHI Conference on Human Factors in Computing Systems* (Hamburg, Germany) *(CHI '23)*. Association for Computing Machinery, New York, NY, USA, Article 626, 14 pages. https://doi.org/10.1145/3544548.3581361

[4] Luis M Alves, Rafael M Afonso, Patric T Pereira, and Paulo AF Martins. 2021. Double-sided self-pierce riveting of dissimilar materials. *The International Journal of Advanced Manufacturing Technology* 115, 11-12 (2021), 3679–3687.

[5] Kristin Angel, Harvey H Tsang, Sarah S Bedair, Gabriel L Smith, and Nathan Lazarus. 2018. Selective electroplating of 3D printed parts. *Additive Manufacturing* 20 (2018), 164–172.

[6] Abul Al Arabi, Jiahao Li, Xiang 'Anthony Chen, and Jeeeun Kim. 2022. Mobiot: Augmenting Everyday Objects into Moving IoT Devices Using 3D Printed Attachments Generated by Demonstration. In *Proceedings of the 2022 CHI Conference on Human Factors in Computing Systems* (New Orleans, LA, USA) *(CHI '22)*. Association for Computing Machinery, New York, NY, USA, Article 273, 14 pages. https://doi.org/10.1145/3491102.3517645

[7] Bambu. September 14, 2023. https://bambulab.cn/zh-cn

[8] Juraj Beniak, L'ubomír Šooš, Peter Križan, Miloš Matúš, and Vít Ruprich. 2022. Resistance and strength of conductive PLA processed by FDM additive manufacturing. *Polymers* 14, 4 (2022), 678.

[9] Dustin Beyer, Serafima Gurevich, Stefanie Mueller, Hsiang-Ting Chen, and Patrick Baudisch. 2015. Platener: Low-Fidelity Fabrication of 3D Objects by Substituting 3D Print with Laser-Cut Plates. In *Proceedings of the 33rd Annual ACM Conference on Human Factors in Computing Systems* (Seoul, Republic of Korea) *(CHI '15)*. Association for Computing Machinery, New York, NY, USA, 1799–1806. https://doi.org/10.1145/2702123.2702225

[10] Caio Brito, Gutenberg Barros, Walter Correia, Veronica Teichrieb, and João Marcelo Teixeira. 2016. Multimodal Augmentation of Surfaces Using Conductive 3D Printing. In *ACM SIGGRAPH 2016 Posters* (Anaheim, California) *(SIGGRAPH '16)*. Association for Computing Machinery, New York, NY, USA, Article 15, 2 pages. https://doi.org/10.1145/2945078.2945093

[11] Jinwei Cao, Xin Li, Yiwei Liu, Guang Zhu, and Run-Wei Li. 2023. Liquid metal-based electronics for on-skin healthcare. *Biosensors* 13, 1 (2023), 84.

[12] A Fassler and C Majidi. 2013. Soft-matter capacitors and inductors for hyperelastic strain sensing and stretchable electronics. *Smart Materials and Structures* 22, 5 (2013), 055023.

[13] Shuyue Feng, Cheng Yao, Weijia Lin, Jiayu Yao, Chao Zhang, Zhongyu Jia, Lijuan Liu, Masulani Bokola, Hangyue Chen, Fangtian Ying, and Guanyun Wang. 2023. MechCircuit: Augmenting Laser-Cut Objects with Integrated Electronics, Mechanical Structures and Magnets. In *Proceedings of the 2023 CHI Conference on Human Factors in Computing Systems* (Hamburg, Germany) *(CHI '23)*. Association for Computing Machinery, New York, NY, USA, Article 735, 15 pages. https://doi.org/10.1145/3544548.3581002

[14] Patrick F Flowers, Christopher Reyes, Shengrong Ye, Myung Jun Kim, and Benjamin J Wiley. 2017. 3D printing electronic components and circuits with conductive thermoplastic filament. *Additive Manufacturing* 18 (2017), 156–163.

[15] Naila Gasanova Naila Gasanova. 2023. Research on the technology of preparing plastic and threaded components using 3d printing or additive manufacturing. *Equipment, Technologies, Materials* (2023). https://doi.org/10.36962/etm14022023-154

[16] Jun Gong, Olivia Seow, Cedric Honnet, Jack Forman, and Stefanie Mueller. 2021. MetaSense: Integrating Sensing Capabilities into Mechanical Metamaterial. In *The 34th Annual ACM Symposium on User Interface Software and Technology* (Virtual Event, USA) *(UIST '21)*. Association for Computing Machinery, New York, NY, USA, 1063–1073. https://doi.org/10.1145/3472749.3474806

[17] Daniel Groeger and Jürgen Steimle. 2018. ObjectSkin: augmenting everyday objects with hydroprinted touch sensors and displays. *Proceedings of the ACM on Interactive, Mobile, Wearable and Ubiquitous Technologies* 1, 4 (2018), 1–23.

[18] Daniel Groeger and Jürgen Steimle. 2019. LASEC: Instant Fabrication of Stretchable Circuits Using a Laser Cutter. In *Proceedings of the 2019 CHI Conference on Human Factors in Computing Systems* (Glasgow, Scotland Uk) *(CHI '19)*. Association for Computing Machinery, New York, NY, USA, 1–14. https://doi.org/10.1145/3290605.3300929

[19] Jianzhe Gu, David E Breen, Jenny Hu, Lifeng Zhu, Ye Tao, Tyson Van de Zande, Guanyun Wang, Yongjie Jessica Zhang, and Lining Yao. 2019. Geodesy: Self-rising 2.5 d tiles by printing along 2d geodesic closed path. In *Proceedings of the 2019 CHI Conference on Human Factors in Computing Systems*. 1–10.

[20] Freddie Hong, Connor Myant, and David E Boyle. 2021. Thermoformed Circuit Boards: Fabrication of Highly Conductive Freeform 3D Printed Circuit Boards with Heat Bending. In *Proceedings of the 2021 CHI Conference on Human Factors in Computing Systems* (Yokohama, Japan) *(CHI '21)*. Association for Computing Machinery, New York, NY, USA, Article 669, 10 pages. https://doi.org/10.1145/3411764.3445469

[21] Syed Fouzan Iftekar, Abdul Aabid, Adibah Amir, and Muneer Baig. 2023. Advancements and Limitations in 3D Printing Materials and Technologies: A Critical Review. *Polymers* 15, 11 (2023), 2519.

[22] Qi Jiang, Peilei Zhang, Zhishui Yu, Haichuan Shi, Di Wu, Hua Yan, Xin Ye, Qinghua Lu, and Yingtao Tian. 2021. A review on additive manufacturing of pure copper. *Coatings* 11, 6 (2021), 740.

[23] R. Jockwer, G. Fink, and J. Köhler. 2018. Assessment of the failure behaviour and reliability of timber connections with multiple dowel-type fasteners. *Engineering Structures* (2018). https://doi.org/10.1016/J.ENGSTRUCT.2018.05.081

[24] Yun Hee Ju, Hee-Jin Lee, Chul Jong Han, Cheul-Ro Lee, Youngmin Kim, and Jong-Woong Kim. 2020. Pressure-sensitive adhesive with controllable adhesion for fabrication of ultrathin soft devices. *ACS Applied Materials & Interfaces* 12, 36 (2020), 40794–40801.

[25] Nikos Karathanasopoulos, Kedar S Pandya, and Dirk Mohr. 2021. Self-piercing riveting process: prediction of joint characteristics through finite element and neural network modeling. *Journal of Advanced Joining Processes* 3 (2021), 100040.

[26] Kunihiro Kato, Kaori Ikematsu, and Yoshihiro Kawahara. 2020. CAPath: 3D-Printed Interfaces with Conductive Points in Grid Layout to Extend Capacitive Touch Inputs. *Proc. ACM Hum.-Comput. Interact.* 4, ISS, Article 193 (nov 2020), 17 pages. https://doi.org/10.1145/3427321

[27] Yoshihiro Kawahara, Steve Hodges, Benjamin S Cook, Cheng Zhang, and Gregory D Abowd. 2013. Instant inkjet circuits: lab-based inkjet printing to support rapid prototyping of UbiComp devices. In *Proceedings of the 2013 ACM international joint conference on Pervasive and ubiquitous computing*. 363–372.

[28] Dong Seok Kim, Jae-Min Jeong, Hong Jun Park, Yeong Kyun Kim, Kyoung G Lee, and Bong Gill Choi. 2021. Highly concentrated, conductive, defect-free graphene ink for screen-printed sensor application. *Nano-micro letters* 13 (2021), 1–14.

[29] Joohyung Kim, Alexander Alspach, and Katsu Yamane. 2017. Snapbot: A reconfigurable legged robot. In *2017 IEEE/RSJ International Conference on Intelligent Robots and Systems (IROS)*. IEEE, 5861–5867. https://doi.org/10.1109/IROS.2017.8206477

[30] Myung Jun Kim, Mutya A Cruz, Shengrong Ye, Allen L Gray, Gabriel L Smith, Nathan Lazarus, Christopher J Walker, Hjalti H Sigmarsson, and Benjamin J Wiley. 2019. One-step electrodeposition of copper on conductive 3D printed objects. *Additive Manufacturing* 27 (2019), 318–326.

[31] Donghyeon Ko, Yoonji Kim, Junyi Zhu, Michael Wessely, and Stefanie Mueller. 2023. FlexBoard: A Flexible Breadboard for Interaction Prototyping on Curved and Deformable Surfaces. In *Proceedings of the 2023 CHI Conference on Human Factors in Computing Systems* (Hamburg, Germany) *(CHI '23)*. Association for Computing Machinery, New York, NY, USA, Article 733, 13 pages. https://doi.org/10.1145/3544548.3580748

[32] Yoichiro Koga and Akira Todoroki. 2019. Three-dimensionally printed designable joint for carbon fibre reinforced plastics. *Advanced Composite Materials* 28, 2 (2019), 147–161.

[33] Roman Koleňák, Igor Kostolnỳ, Jaromír Drápala, Martin Kusỳ, and Matej Pašák. 2019. Research on soldering AlN ceramics with Cu substrate using Sn-Ag-Ti solder. *Soldering & Surface Mount Technology* 31, 2 (2019), 93–101.

[34] Robert Kovacs. 2021. Human-Scale Personal Fabrication. In *Adjunct Proceedings of the 34th Annual ACM Symposium on User Interface Software and Technology* (Virtual Event, USA) *(UIST '21 Adjunct)*. Association for Computing Machinery, New York, NY, USA, 162–165. https://doi.org/10.1145/3474349.3477588

[35] Robert Kovacs, Anna Seufert, Ludwig Wall, Hsiang-Ting Chen, Florian Meinel, Willi Müller, Sijing You, Maximilian Brehm, Jonathan Striebel, Yannis Kommana, Alexander Popiak, Thomas Bläsius, and Patrick Baudisch. 2017. TrussFab: Fabricating Sturdy Large-Scale Structures on Desktop 3D Printers. In *Proceedings of the 2017 CHI Conference on Human Factors in Computing Systems* (Denver, Colorado, USA) *(CHI '17)*. Association for Computing Machinery, New York, NY, USA, 2606–2616. https://doi.org/10.1145/3025453.3026016

[36] Xiang Li, Xing Su, and Yunhui Liu. 2017. Cooperative robotic soldering of flexible PCBs. In *2017 IEEE/RSJ International Conference on Intelligent Robots and Systems (IROS)*. 1651–1656. https://doi.org/10.1109/IROS.2017.8205975

[37] Bingheng Lu, Hongbo Lan, and Hongzhong Liu. 2018. Additive manufacturing frontier: 3D printing electronics. *Opto-Electronic Advances* 1, 1 (2018), 170004.

[38] Shunqi Mei, Jian Wang, Jitao Wan, and Xichun Wu. 2023. Preparation Methods and Properties of CNT/CF/G Carbon-Based Nano-Conductive Silicone Rubber. *Applied Sciences* 13, 11 (2023), 6726.

[39] Steven Nagels, Raf Ramakers, Kris Luyten, and Wim Deferme. 2018. Silicone Devices: A Scalable DIY Approach for Fabricating Self-Contained Multi-Layered Soft Circuits Using Microfluidics. In *Proceedings of the 2018 CHI Conference on Human Factors in Computing Systems* (Montreal QC, Canada) *(CHI '18)*. Association for Computing Machinery, New York, NY, USA, 1–13. https://doi.org/10.1145/3173574.3173762

[40] Marla Narazani, Chloe Eghtebas, Gudrun Klinker, Sarah L. Jenney, Michael Mühlhaus, and Frank Petzold. 2019. Extending AR Interaction through 3D Printed Tangible Interfaces in an Urban Planning Context. In *Adjunct Proceedings of the 32nd Annual ACM Symposium on User Interface Software and Technology* (New Orleans, LA, USA) *(UIST '19 Adjunct)*. Association for Computing Machinery, New York, NY, USA, 116–118. https://doi.org/10.1145/3332167.3356891

[41] Jonas Neubert, Arne Rost, and Hod Lipson. 2014. Self-soldering connectors for modular robots. *IEEE Transactions on Robotics* 30, 6 (2014), 1344–1357.

[42] Simon Olberding, Sergio Soto Ortega, Klaus Hildebrandt, and Jürgen Steimle. 2015. Foldio: Digital Fabrication of Interactive and Shape-Changing Objects With Foldable Printed Electronics. In *Proceedings of the 28th Annual ACM Symposium on User Interface Software & Technology* (Charlotte, NC, USA) *(UIST '15)*. Association for Computing Machinery, New York, NY, USA, 223–232. https://doi.org/10.1145/2807442.2807494

[43] Simon Olberding, Michael Wessely, and Jürgen Steimle. 2014. PrintScreen: Fabricating Highly Customizable Thin-Film Touch-Displays. In *Proceedings of the 27th Annual ACM Symposium on User Interface Software and Technology* (Honolulu, Hawaii, USA) *(UIST '14)*. Association for Computing Machinery, New York, NY, USA, 281–290. https://doi.org/10.1145/2642918.2647413

[44] Keunwoo Park, Conrad Lempert, Muhammad Abdullah, Shohei Katakura, Jotaro Shigeyama, Thijs Roumen, and Patrick Baudisch. 2022. FoolProofJoint: Reducing Assembly Errors of Laser Cut 3D Models by Means of Custom Joint Patterns. In *Proceedings of the 2022 CHI Conference on Human Factors in Computing Systems* (New Orleans, LA, USA) *(CHI '22)*. Association for Computing Machinery, New York, NY, USA, Article 271, 12 pages. https://doi.org/10.1145/3491102.3501919

[45] C Varun Perumal and Daniel Wigdor. 2015. Printem: instant printed circuit boards with standard office printers inks. In *Proceedings of the 28th Annual ACM Symposium on User Interface Software &# 38; Technology (UIST'15)*. 243–251.

[46] Narjes Pourjafarian, Marion Koelle, Fjolla Mjaku, Paul Strohmeier, and Jürgen Steimle. 2022. Print-A-Sketch: A Handheld Printer for Physical Sketching of Circuits and Sensors on Everyday Surfaces. In *Proceedings of the 2022 CHI Conference on Human Factors in Computing Systems* (New Orleans, LA, USA) *(CHI '22)*. Association for Computing Machinery, New York, NY, USA, Article 270, 17 pages. https://doi.org/10.1145/3491102.3502074

[47] Xinbin Qiu, Xiaomin Zhao, Feixiang Liu, Songlin Chen, Jianfeng Xu, and Guohua Chen. 2019. Surfactant-free carbon black@ graphene conductive ink for flexible electronics. *Journal of Materials Science* 54 (2019), 11157–11167.

[48] Gabriel Saada, Michael Layani, Avi Chernevousky, and Shlomo Magdassi. 2017. Hydroprinting conductive patterns onto 3D structures. *Advanced Materials Technologies* 2, 5 (2017), 1600289.

[49] Martin Schmitz, Jan Riemann, Florian Müller, Steffen Kreis, and Max Mühlhäuser. 2021. Oh, Snap! A Fabrication Pipeline to Magnetically Connect Conventional and 3D-Printed Electronics. In *Proceedings of the 2021 CHI Conference on Human Factors in Computing Systems* (Yokohama, Japan) *(CHI '21)*. Association for Computing Machinery, New York, NY, USA, Article 420, 11 pages. https://doi.org/10.1145/3411764.3445641

[50] Peng Song, Zhongqi Fu, Ligang Liu, and Chi-Wing Fu. 2015. Printing 3D objects with interlocking parts. *Computer Aided Geometric Design* 35 (2015), 137–148.

[51] sphero. September 14, 2023. https://sphero.com/products/bitsnaps

[52] John Steuben, Douglas L Van Bossuyt, and Cameron Turner. 2015. Design for fused filament fabrication additive manufacturing. In *International Design Engineering Technical Conferences and Computers and Information in Engineering Conference*, Vol. 57113. American Society of Mechanical Engineers, V004T05A050.

[53] Saiganesh Swaminathan, Kadri Bugra Ozutemiz, Carmel Majidi, and Scott E. Hudson. 2019. FiberWire: Embedding Electronic Function into 3D Printed Mechanically Strong, Lightweight Carbon Fiber Composite Objects. In *Proceedings of the 2019 CHI Conference on Human Factors in Computing Systems* (Glasgow, Scotland Uk) *(CHI '19)*. Association for Computing Machinery, New York, NY, USA, 1–11. https://doi.org/10.1145/3290605.3300797

[54] Maddux Sy, Sean Fleuriel, Confesol Rodriguez, Kesheng Feng, Robert Moon, Dolores Cruz, and Jon Hander. 2022. RDL Copper Plating Process for Panel Level Packaging Application. In *2022 17th International Microsystems, Packaging, Assembly and Circuits Technology Conference (IMPACT)*. 1–4. https://doi.org/10.1109/IMPACT56280.2022.9966645

[55] Rundong Tian, Sarah Sterman, Ethan Chiou, Jeremy Warner, and Eric Paulos. 2018. MatchSticks: Woodworking through Improvisational Digital Fabrication. In *Proceedings of the 2018 CHI Conference on Human Factors in Computing Systems* (Montreal QC, Canada) *(CHI '18)*. Association for Computing Machinery, New York, NY, USA, 1–12. https://doi.org/10.1145/3173574.3173723

[56] This to That. September 14, 2023. https://thistothat.com/

[57] Nobuyuki Umetani and Ryan Schmidt. 2017. SurfCuit: surface-mounted circuits on 3D prints. *IEEE computer graphics and applications* 37, 3 (2017), 52–60.

[58] Dmitry S Vorunichev. 2021. Application of Additive Technology for 3D Printing of Electronic Devices as a Way to Reduce Prototyping Time. In *2021 International Conference on Quality Management, Transport and Information Security, Information Technologies (IT&QM&IS)*. IEEE, IEEE, 480–483.

[59] Xizi Wan, Zhen Gu, Feilong Zhang, Dezhao Hao, Xi Liu, Bing Dai, Yongyang Song, and Shutao Wang. 2019. Asymmetric Janus adhesive tape prepared by interfacial hydrosilylation for wet/dry amphibious adhesion. *NPG Asia Materials* 11, 1 (2019), 49.

[60] Guanyun Wang, Tingyu Cheng, Youngwook Do, Humphrey Yang, Ye Tao, Jianzhe Gu, Byoungkwon An, and Lining Yao. 2018. Printed paper actuator: A low-cost reversible actuation and sensing method for shape changing interfaces. In *Proceedings of the 2018 CHI Conference on Human Factors in Computing Systems*. 1–12.

[61] Guanyun Wang, Fang Qin, Haolin Liu, Ye Tao, Yang Zhang, Yongjie Jessica Zhang, and Lining Yao. 2020. MorphingCircuit: An Integrated Design, Simulation, and Fabrication Workflow for Self-Morphing Electronics. *Proc. ACM Interact. Mob. Wearable Ubiquitous Technol.* 4, 4, Article 157 (dec 2020), 26 pages. https://doi.org/10.1145/3432232

[62] Guanyun Wang, Humphrey Yang, Zeyu Yan, Nurcan Gecer Ulu, Ye Tao, Jianzhe Gu, Levent Burak Kara, and Lining Yao. 2018. 4DMesh: 4D printing morphing non-developable mesh surfaces. In *Proceedings of the 31st Annual ACM Symposium on User Interface Software and Technology*. 623–635.

[63] Mark Weiser. 1999. The computer for the 21st century. *ACM SIGMOBILE mobile computing and communications review* 3, 3 (1999), 3–11.

[64] Michael Wessely, Ticha Sethapakdi, Carlos Castillo, Jackson C. Snowden, Ollie Hanton, Isabel P. S. Qamar, Mike Fraser, Anne Roudaut, and Stefanie Mueller. 2020. Sprayable User Interfaces: Prototyping Large-Scale Interactive Surfaces with Sensors and Displays. In *Proceedings of the 2020 CHI Conference on Human Factors in Computing Systems* (Honolulu, HI, USA) *(CHI '20)*. Association for Computing Machinery, New York, NY, USA, 1–12. https://doi.org/10.1145/3313831.3376249

[65] Michael Wessely, Theophanis Tsandilas, and Wendy E. Mackay. 2016. Stretchis: Fabricating Highly Stretchable User Interfaces. In *Proceedings of the 29th Annual Symposium on User Interface Software and Technology* (Tokyo, Japan) *(UIST '16)*. Association for Computing Machinery, New York, NY, USA, 697–704. https://doi.org/10.1145/2984511.2984521

[66] Jinliang Wu, Chao Chen, Yawen Ouyang, Denglin Qin, and Haijun Li. 2021. Recent development of the novel riveting processes. *The International Journal of Advanced Manufacturing Technology* 117 (2021), 19–47.

[67] Ke Yan, Jiean Li, Lijia Pan, and Yi Shi. 2020. Inkjet printing for flexible and wearable electronics. *Apl Materials* 8, 12 (2020).

[68] Zeyu Yan, Jiasheng Li, Zining Zhang, and Huaishu Peng. 2024. SolderlessPCB: Reusing Electronic Components in PCB Prototyping through Detachable 3D Printed Housings. In *Proceedings of the CHI Conference on Human Factors in Computing Systems*. 1–17.

[69] Zeyu Yan, Anup Sathya, Sahra Yusuf, Jyh-Ming Lien, and Huaishu Peng. 2022. Fibercuit: Prototyping High-Resolution Flexible and Kirigami Circuits with a Fiber Laser Engraver. In *Proceedings of the 35th Annual ACM Symposium on User Interface Software and Technology*. 1–13.

[70] Zhongjie Zhao, Xiaosu Yi, and G. Xian. 2017. Fabricating structural adhesive bonds with high electrical conductivity. *International Journal of Adhesion and Adhesives* 74 (2017), 70–76. https://doi.org/10.1016/J.IJADHADH.2017.01.002

[71] Clement Zheng, Bo Han, Xin Liu, Laura Devendorf, Hans Tan, and Ching Chiuan Yen. 2023. Crafting Interactive Circuits on Glazed Ceramic Ware. In *Proceedings of the 2023 CHI Conference on Human Factors in Computing Systems* (Hamburg, Germany) *(CHI '23)*. Association for Computing Machinery, New York, NY, USA, Article 474, 18 pages. https://doi.org/10.1145/3544548.3580836

[72] Junyi Zhu, Lotta-Gili Blumberg, Yunyi Zhu, Martin Nisser, Ethan Levi Carlson, Xin Wen, Kevin Shum, Jessica Ayeley Quaye, and Stefanie Mueller. 2020. CurveBoards: Integrating Breadboards into Physical Objects to Prototype Function in the Context of Form. In *Proceedings of the 2020 CHI Conference on Human Factors in Computing Systems* (Honolulu, HI, USA) *(CHI '20)*. Association for Computing Machinery, New York, NY, USA, 1–13. https://doi.org/10.1145/3313831.3376617